Ion Beam Analyses of Carbon Nanotubes

Fabian U. Naab,* Orin W. Holland, Jerome L. Duggan, and Floyd D. McDaniel

Ion Beam Modification and Analysis Laboratory, Department of Physics, P.O. Box 311427, University of North Texas, Denton, Texas 76203-1427

Received: August 30, 2004; In Final Form: November 1, 2004

The utility of ion beam analysis (IBA) techniques to quantitatively determine impurities in carbon nanotubes (CNTs) over a wide range of atomic numbers is demonstrated. Such techniques have not previously been used to monitor impurities and their effects in this unique material. Despite the difficulty in mounting the samples (which generally are formed into a powdery aggregate rather in a thin film), it is shown that reliable and accurate measurements of impurity concentrations can be achieved. Particle-induced X-ray emission (PIXE) and elastic recoil detection (ERD) analyses were used to characterize both metallic and very light (e.g., hydrogen) impurities in CNTs. This paper reports the first direct measurement of hydrogen in CNTs using an IBA technique. This is significant because CNTs are being actively investigated for hydrogen storage technology for energy applications.

Introduction

Carbon nanotubes (CNTs) were discovered in 1991 by Iijima.[1] They are long, thin cylinders of carbon that can be thought of as a sheet of graphite (a hexagonal lattice of carbon) rolled into a cylinder. These unique macromolecules exhibit remarkable physical and electrical properties. The properties depend on the different varieties of nanotube (defined by its diameter, length, and chirality), as well as the number of walls that comprise the tube. A tube consisting of a single cylindrical wall is referred to as a single-walled nanotube (SWNT), whereas multiwalled nanotubes (MWNTs) consist of an array of cylinders inside other cylinders. A double-walled nanotube (DWNT) is a multiwalled tube consisting of only two cylindrical walls. Carbon nanotubes are ultrastrong, elastic, and durable. The measured elastic strength of SWNTs, i.e., Young's modulus, has yielded a value close to 1 TPa, which is approximately 5 times larger than the value for steel.[2] Also, CNTs have unique electronic properties. They can behave either as a metal or a semiconductor. (For example, see http://www.ugc.edu.hk/rgc/rgcnews3/Pages/Nano1-EN.html and http://www.aip.org/png/html/nanotube.htm.)

Contaminants can greatly influence the measured properties of CNTs (as in other materials), making it difficult to determine intrinsic effects. Commercially available CNTs contain substantial amounts of impurities including metals, introduced intentionally as a catalyst during growth, and carbonaceous material other than nanotubes. Alternatively, impurities such as hydrogen in CNTs have been intentionally introduced to determine the potential of CNTs for use in a hydrogen storage technology. Because hydrogen has great potential as an energy source, an efficient storage medium is required before hydrogen becomes useful in energy applications. The unique architecture of CNTs makes them potentially the best carbon-based absorbent for hydrogen. Several research groups have reported storage capacities of ∼4 wt % in SWNTs. Unfortunately, these results have not been reproducible, partly because of lack of control in the synthesis of the SWNTs and the ambiguity in the monitoring process for hydrogen absorption/desorption.

It is clear that impurities and their effects in CNTs are an important area of interest in the understanding and commercialization of this unique material. To this end, we have used a variety of ion beam analysis (IBA) techniques to characterize CNTs. To our knowledge, this is the first report detailing the analyses of this material using IBA techniques. Particle-induced X-ray emission (PIXE) analysis was done to identify impurities and their concentrations in the various samples. PIXE is sensitive to impurities with atomic number ≥ 12, which includes most metallic impurities found in CNTs. PIXE measurements were done in different forms of CNTs including SWNTs, DWNTs, and MWNTs, as well as material from different vendors. Additionally, direct measurements of hydrogen using elastic recoil detection analysis (ERDA) were performed. This is the first report of a direct measurement of hydrogen in CNTs. Other techniques, such as weight analysis, residual gas analysis, etc., do not directly measure hydrogen but rather measure another parameter that must be related to the amount of stored hydrogen. Application of a direct measuring technique such as ERDA has the potential to resolve some of the ambiguities in the monitoring process for hydrogen absorption and release in CNTs.

PIXE Analysis

PIXE is a well-established analytical method for multielemental determination that is based on ion bombardment to produce characteristic X-rays of the elements present in the material.[3]

In the present experiment, samples were irradiated with 1.5 MeV protons using a 2.5 MV van de Graaff accelerator at the University of North Texas. As shown in Figure 1, the HPGe X-ray detector was positioned at a backscattering angle $\theta = 145°$, and the beam's incident angle on the sample was $\alpha = 17°$. Samples were electrically insulated and biased at +300 V to collect secondary electrons during current integration, which is used for determining the number of incident protons on the sample (N_p) during spectral acquisition.

Because electronic excitation occurs along much of the ion range, the total X-ray yield is a result of depth-dependent factors

* Corresponding author. E-mail: fun001@unt.edu.

10.1021/jp040592y CCC: $30.25 © 2005 American Chemical Society
Published on Web 01/07/2005

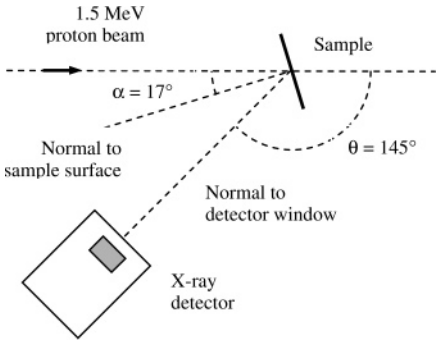

Figure 1. Experimental setup used for the PIXE measurements.

that must be integrated to yield the average impurity concentration in the bulk. The average mass concentration for each element is therefore given for every measurable element by the following expression

$$C_Z = \frac{N_X A_Z}{\epsilon_Z b_Z N_p \int_{E_0}^{0} \frac{\sigma_Z(E)\, T_Z(E)}{S_M(E)}\, dE} \quad (1)$$

where N_X is the number of counts for the K_α or L_α transition in the X-ray spectrum, A_Z is atomic mass of the element, ϵ_Z is the detector's absolute efficiency for the K_α or L_α transition, b_Z is the intensity fraction of the K_α or L_α transition,[4] N_p is the number of incident protons, σ_Z is the elemental K-shell or L-shell X-ray production cross section, T_Z is the transmission in the sample for the K_α or L_α X-ray, and S_M is the stopping power of the matrix of the sample. The transmission factor determines the attenuation of the X-rays along the outward path originating from within the sample to the detector. This factor is given by $T_Z = e^{-\mu(E)\delta x}$, where $\mu(E)$ is the mass attenuation coefficient for the characteristic X-ray of energy E, δ is the sample density, and x is the length that the X-rays travel in the sample.

The evaluation of the integral in eq 1 requires that values of the various parameters be obtained. To this end, the AXIL code[5] was first used to fit the spectra to extract the area of each peak. Next, it was assumed in the determination of T_Z and S_M that the sample matrix was 100% carbon. Values for the mass attenuation coefficients were obtained from ref 6, and discrete values for S_M and σ_Z were obtained from the SRIM[7] and ISICS[8] codes, respectively. A polynomial function was fitted to each of these sets of values to evaluate eq 1 using Mathcad.

Sample Preparation for PIXE. The CNTs samples were in two forms: powder and small balls of ~1 mm in diameter (buckypearl nanotubes). These materials were sandwiched between two plastic foils: 8.5-μm-thick Kapton foil on one side and 0.15-μm-thick AP1 Moxtek[9] film on the another side. Each foil was mounted on an aluminum frame. The beam entered the sample through the Moxtek film. The Moxtek frame was covered with carbon tape to avoid characteristic X-ray production due to the scattered beam. Secondary X-ray fluorescence in the frames was completely negligible. The Moxtek films were 25 μg/cm^2, which is thin enough to avoid corrections due to beam energy loss and X-ray attenuation. These films are also virtually free of contaminants. Only a small number of Fe K X-rays were introduced by the Moxtek film in each spectrum, which is completely negligible compared to the number of Fe K X-rays coming from the sample.

X-ray Detector Efficiency. The efficiency of the X-ray detector was determined using 18 K_α transitions of different elements prepared as thin targets according to ref 10. These

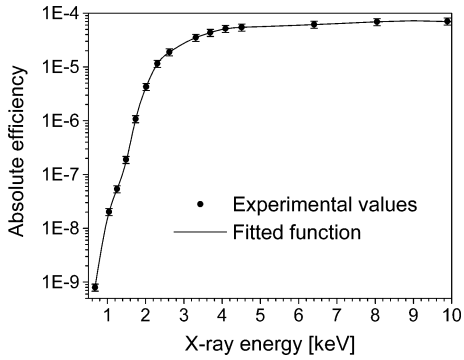

Figure 2. Absolute efficiency curve of the X-ray detector. The efficiency has been measured from 0.667 (F K_α) to 25.27 (Sn K_α) keV. In this plot The values for the K_α transitions of Se, Rh, and Sn are not included in this plot to show with better detail the curve at low energy. The curve remains flat between 10 and 25 keV.

TABLE 1: List of Nanotube Materials Analyzed Using PIXE

material	i.d. (nm)	o.d. (avg.) (nm)	length (μm)
SWNTs[a]		0.8−2 (1.1)	0.5−100
buckypearls[b]		1−1.5	
DWNTs[a]	1.3−2.0	<5	0.5−50
MWNTs[a]	5−10	60−100	0.5−50

[a] Vendor: Nanostructured & Amorphous Materials, Inc. (www.nanoamor.com). [b] Carbon Nanotechnologies, Inc.

measurements were done using a 1.5 MeV $^4He^{+1}$ beam. The experimental setup was the same as the one shown in Figure 1 but with the addition of a surface barrier detector (SBD) placed at an angle of 150° to the beam direction (opposite to the X-ray detector). The X-ray excitation and Rutherford backscattered (RBS) spectra were taken simultaneously to evaluate the detector's absolute efficiency independently of the target thickness and the total ion fluence. The efficiency for each K transition was calculated using the formula

$$\epsilon_Z = \frac{N_X \Delta\Omega \sigma_R}{N_R b_Z \sigma_X} \quad (2)$$

where N_X is the number of counts corresponding to the K_α transition in the X-ray spectrum, N_R is the number of counts in the RBS spectrum for the corresponding element, $\Delta\Omega$ is the solid angle of the SBD, σ_R is the RBS cross section,[11] σ_X is the X-ray production cross section for the K shell,[12,13] and b_Z is the intensity fraction of the K_α transition.[4] A polynomial fit was done using *lspline* and *interp* functions of Mathcad 8.0 to the natural logarithm of the experimental values. The efficiency curve is shown in Figure 2.

PIXE Results. Table 1 lists the nanotube materials analyzed using PIXE and some of their characteristics. Figure 3 shows the PIXE spectrum for the sample labeled as SWNT (1.4 nm) in Figure 4a.

The PIXE results are summarized in Figure 4a for the SWNTs used in this study (see Table 1). The bar graph in the figure gives the mass concentration as a function of the various elements detected in the samples. The results show that all of the SWNTs (independent of vendor and average size) contain large amounts (~9% or less) of metallic impurities. Elemental variations among the various types of SWNTS are mainly due to the different catalytic materials used by the vendors during growth. Despite these variations, the total amount of metallic impurities given on the right side of the figure is nearly the same in all of the SWNTs samples. Figure 4b gives the impurity

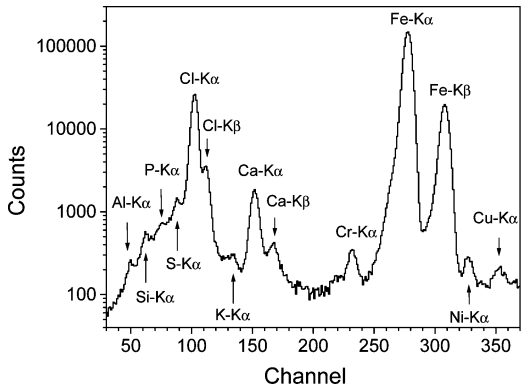

Figure 3. X-ray spectrum for SWNTs (1.4 nm).

concentrations in the different types of nanotubes (SWNTs, DWNTs, and MWNTs), as well as graphite. Significant differences are observed in these samples. It is clear that both SWNTs and DWNTs contain substantially more metallic impurities than either MWNTs or graphite.

The Nanostructured & Amorphous Materials, Inc., Web page (www.nanoamor.com) shows the certificate of analysis for some of the impurities we have detected in the CNT samples. Although our results are in very good agreement with their analysis, the PIXE results indicated a number of other impurities that were not reported in their certificate of analysis.

ERD Analysis

Elastic recoil detection[14−17] (ERD) is an IBA technique for quantitative analysis of light elements in solids. The sample to be analyzed is irradiated with an ion beam (e.g., He, C, or O ions) of several megaelectronvolts. Light elements (e.g., H, D) from the sample are scattered in the forward directions through nuclear interactions between the incident ions and the atoms in the sample. The recoil ions are detected with an SBD. From the measured energy spectrum of the recoils, a concentration depth profile can be calculated.[18−20] The detection of scattered ions from the incident ion beam is normally suppressed with the use of a stopper foil in front of the detector in order to avoid background. Because the stopper foil is thick enough to stop the scattered beam, the recoils heavier than the mass of the beam ions will also be stopped. For low ion energies (<0.3 MeV/amu), the scattering cross section can be calculated assuming Rutherford scattering. For higher energies, experimentally measured cross sections have to be used in most cases. The accuracy of this technique (∼10%) is limited by the uncertainties in the stopping power values of the sample material, experimental cross-section values, and geometrical uncertainties.

The ERD measurements were done using the same beam line as used for the PIXE measurements. The experimental setup is shown in Figure 5. The 1.7 MeV $^4He^{+1}$ beam struck the sample with an incident angle of 75°. The scattered hydrogen ions were detected with an SBD at 30° to the beam direction. A 7.5 μm Mylar foil was used to filter out the scattered beam and heavier scattered elements from the sample. The beam current on the sample was ∼20 nA.

The hydrogen spectra were analyzed using the SIMNRA code.[21,22] SIMNRA is a program for the simulation of back- and forward-scattering spectra for ion beam analysis with megaelectronvolt ions. SIMNRA is mainly intended for the simulation of spectra with non-Rutherford backscattering cross sections, nuclear reactions, and ERD analysis.

The results were normalized using a tungsten mesh, which has an open area of 77.4% and wire diameter of 0.0015-in. according to vendor specifications. This mesh is placed upstream at ∼70 cm from the target and is electrically insulated. A fraction of the beam interacts with the mesh producing a net current that is integrated by a current integrator. The mesh is inside a cylinder biased at −300 V to avoid electrons escaping from the mesh. Our test indicates that this voltage is adequate to suppress all secondary electrons. The cylinder axis is along the beam line and a hole at each base allows the beam to pass through. Under these conditions, the mesh produced a current that was 25% of the beam current on the target.

A Kapton film was used as the hydrogen standard to normalize the results. A Kapton film was irradiated several times before and after the sample measurements to check beam stability and reproducibility of the data. For each measurement, a new Kapton foil was used.

Sample Preparation for ERD. The samples that were analyzed are listed in Table 2. Each sample was sealed to a silicon wafer, and the silicon wafer was mounted on a rotatable

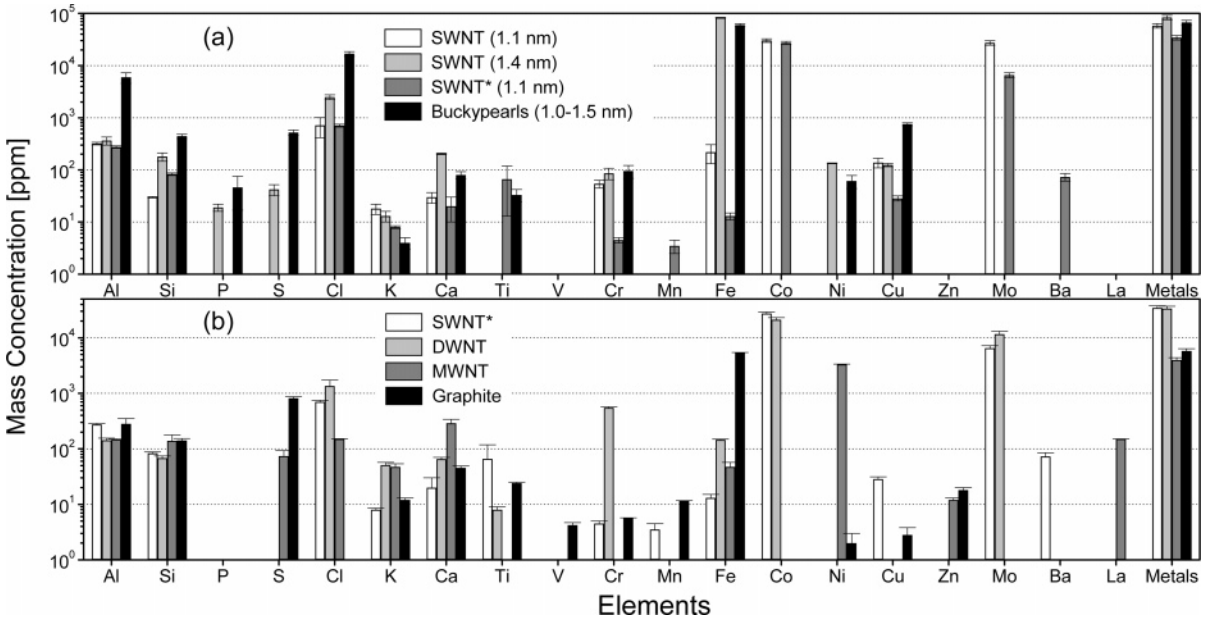

Figure 4. Mass concentrations of those elements found in various CNTs and graphite.

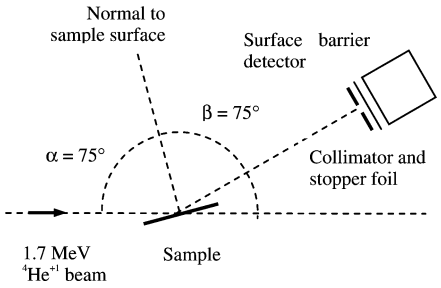

Figure 5. Experimental setup used for the ERD measurements.

TABLE 2: List of Materials Analyzed Using the ERD Technique and Their Hydrogen Weight Concentrations

material	concentration (%)
SWNTs[a]	0.031
	0.022
	0.037
	0.036
DWNTs[a]	0.058
MWNTs[a]	0.050
	0.042
	0.033
CNFs[a,b]	0.150
Zyvex film[c]	1.50

[a] Vendor: Nanostructured & Amorphous Materials, Inc. (http://www.nanoamor.com). [b] o.d. = 240−500 nm. [c] Functionalized CNTs. Zyvex Corporation. (http://www.zyvex.com/index.html).

feedthrough to adjust the beam incident angle on the sample. The Zyvex film was held with carbon tape, to the silicon wafer. For the other materials, a silicon wafer was covered with carbon tape and the nanotubes/fibers were evenly spread across it; then the material was pressed with a clean stainless steel scoopula to form a smooth surface. The thickness of the material was sufficient to avoid producing protons on the tape that would reach the detector.

ERD Results. Five spectra were acquired for each sample and standard. Each spectrum was acquired using 1 μC integrated charge through the mesh. For each sample and Kapton standard, we found that the total hydrogen count in the spectrum decreases linearly for each successive run down to ~70% for the fifth run relative to the first one. This effect might be because of diffusion of hydrogen from the beam spot due to a temperature gradient[23] or ion-induced release.[24] To obtain the hydrogen concentration in the sample, the total spectrum corresponding to the five runs was used to decrease the statistical uncertainty. The calculation of the hydrogen concentration for each of the five runs gave the same result. The average hydrogen concentration obtained for the five runs was extrapolated linearly to zero charge to account for the out diffusion of the hydrogen. Figure 6 shows a typical spectrum for the Kapton foil and MWNT sample corresponding to the five spectra added together. Also, Figure 6 shows the SIMNRA simulation to fit each spectrum. The proton elastic recoil cross sections used were those in ref 25.

We used the Kapton spectra to determine the relationship between the integrated charge through the mesh and the number of ions striking the sample multiplied by the detector solid angle. This was done by using the SIMNRA code to match the spectrum and simulation area in the energy range between 150 and 600 keV. For the particular setup and integrated charge for these measurements, the hydrogen weight detection limit was estimated to be ~10 ppm.

The ERD results are shown in Table 2. The different values for the SWNTs and MWNTs correspond to samples from

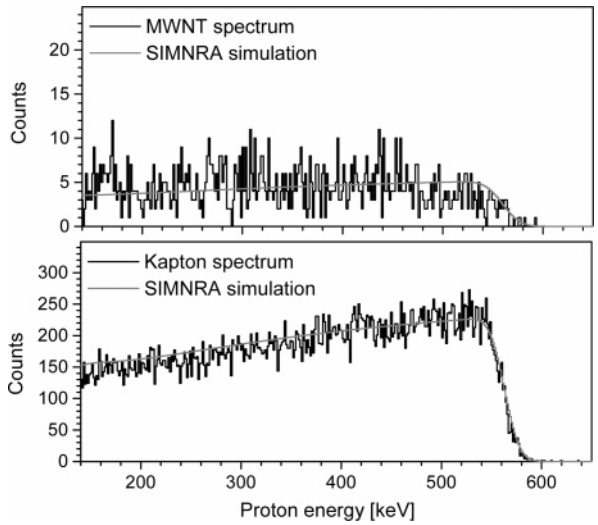

Figure 6. ERD spectra and SIMNRA simulations. Top: Multiwalled carbon nanotube (0.050 wt %, 0.6 at. %). Bottom: Kapton standard (2.62 wt %, 25.6 at. %). The conditions for the simulations are according to the sketch in Figure 5. The stopper foil was 7.5-μm Mylar. Spectrum broadening due to geometrical effects in the experimental setup was included in the simulation program.

different batches. Although the measurements were done only on samples as supplied by the vendor and no attempts were made to absorb additional hydrogen, carbon nanofibers (CNFs, see structural characteristics of this material in ref 26) were found to contain a substantially higher hydrogen concentration (0.15 wt %) than any of the nonfunctionalized CNTs (0.022−0.058 wt %). Although the concentration is well below the targeted concentration established by the Department of Energy of 6.5 wt % (www.energy.gov), the results are encouraging and suggest that this material might offer more potential as a storage medium than the CNTs.

The high hydrogen concentration measured in the Zyvex films (1.5 wt %) is attributed to the binder used to form the nanotubes into a thin film. The Zyvex film is not considered as a viable hydrogen storage medium.

Conclusions

Results of ion beam analyses of different types of CNTs were presented. A variety of analysis techniques are available to provide elemental analyses over an extended range of atomic number including hydrogen. Hydrogen profiling of the CNTs using ERDA provided the first direct measurement of hydrogen in this technologically important material. Such measurements should help in the understanding of hydrogen absorption/desorption in CNTs and lead to optimization of this material for use in hydrogen storage technology.

Acknowledgment. Work at UNT was supported in part by NSF, Texas Advanced Technology Program, and the Robert A. Welch Foundation.

References and Notes

(1) Iijima, S. *Nature* **1991**, *354*, 56.

(2) Dujardin, E.; Ebbesen, T. W.; Krishnan, A.; Yianilos P. N.; Treacy, M. J. *Phys. Rev. B* **1998**, *58*, 14013.

(3) *Particle-Induced X-ray Emission Spectroscopy (PIXE)*; Johansson, S. E., Campbell, J. L., Malmqvist, K. G., Eds.; John Wiley & Sons: New York, 1995.

(4) *Table of Isotopes*; Firestone, R. B., Shirley, V. S., Eds.; John Wiley & Sons: New York, 1996.
(5) Van Espen, P.; Nullens H.; Adams F. *Nucl. Instrum. Methods* **1977**, *142*, 243.
(6) Orlic, I.; Loh, K. K.; Sow, C. H.; Tang, S. M.; Thong, P. *Nucl. Instrum. Methods B* **1993**, *74*, 352.
(7) Ziegler, J. F.; Biersack, J. P.; Littmark, U. *The Stopping and Range of Ions in Solids*; Pergamon Press: New York, 1999.
(8) Liu, Z.; Cipolla S. J. *Comput. Phys. Comm.* **1996**, *97*, 315.
(9) www.moxtek.com.
(10) Lennard, W. N.; Phillips, D. *Nucl. Instrum. Methods* **1979**, *166*, 521.
(11) L'Ecuyer, J.; Davies, J. A.; Matsunami, N. *Nucl. Instrum. Methods* **1979**, *160*, 337.
(12) Brandt, W.; Lapicki, G. *Phys. Rev. A* **1981**, *23*, 1717.
(13) Lapicki, G.; McDaniel, F. D. *Phys. Rev. A* **1980**, *22*, 1896.
(14) L'Ecuyer, J.; Brassard, C.; Cardinal, C.; Chabbal, J.; Deschenes L.; Labrie, J. P. *J. Appl. Phys.* **1976**, *47*, 381.
(15) Doyle, B. L.; Peercy, P. S. *Appl. Phys. Lett.* **1979**, *34*, 811.
(16) Doyle, B. L.; Brice, D. K. *Nucl. Instrum. Methods B* **1988**, *35*, 301.
(17) Composto, R. J.; Walters, R. M.; Genzer, J. *Mater. Sci. Eng. Res.* **2002**, *38*, 107.
(18) Doyle, B. L.; Brice, D. K. *Nucl. Instrum. Methods B* **1988**, *35*, 301.
(19) Turos, A.; Meyer, O. *Nucl. Instrum. Methods B* **1984**, *4*, 92.
(20) Wang, Y.; Liao, C.; Yang, S.; Zheng, Z. *Nucl. Instrum. Methods B* **1990**, *47*, 427.
(21) Mayer, M. *SIMNRA User's Guide*; Report IPP 9/113; Max-Planck-Institut fur Plasmaphysik: Garching, Germany, 1997 (www.rzg.mpg.de/~man).
(22) Mayer, M. In *Proceedings of the 15th International Conference on the Application of Accelerators in Research and Industry*; 1999; Vol. 475, p 541.
(23) Wang, Y. Q. *Nucl. Instrum. Methods B* **2004**, *219*−*220*, 115.
(24) Green, P. F.; Doyle B. L. *Nucl. Instrum. Methods B* **1986**, *18*, 647.
(25) Kim, C.; Kim, S.; Choi, H. *Nucl. Instrum. Methods B* **1999**, *155*, 229.
(26) Chambers, A.; Park, C.; Baker, R. T. K.; Rodriguez, N. M. *J. Phys. Chem. B* **1998**, *102*, 4253.